

# Fermi Large Area Telescope Measurements of the Diffuse Gamma-Ray Emission at Intermediate Galactic Latitudes

A. A. Abdo,<sup>1,2</sup> M. Ackermann,<sup>3</sup> M. Ajello,<sup>3</sup> B. Anderson,<sup>4</sup> W. B. Atwood,<sup>4</sup> M. Axelsson,<sup>5,6</sup> L. Baldini,<sup>7</sup> J. Ballet,<sup>8</sup> G. Barbiellini,<sup>9,10</sup> D. Bastieri,<sup>11,12</sup> B. M. Baughman,<sup>13</sup> K. Bechtol,<sup>3</sup> R. Bellazzini,<sup>7</sup> B. Berenji,<sup>3</sup> R. D. Blandford,<sup>3</sup> E. D. Bloom,<sup>3</sup> E. Bonamente,<sup>14,15</sup> A. W. Borgland,<sup>3</sup> J. Bregeon,<sup>7</sup> A. Brez,<sup>7</sup> M. Brigida,<sup>16,17</sup> P. Bruel,<sup>18</sup> T. H. Burnett,<sup>19</sup> G. A. Caliandro,<sup>16,17</sup> R. A. Cameron,<sup>3</sup> P. A. Caraveo,<sup>20</sup> J. M. Casandjian,<sup>8</sup> C. Cecchi,<sup>14,15</sup> E. Charles,<sup>3</sup> A. Chekhtman,<sup>1,21</sup> C. C. Cheung,<sup>22</sup> J. Chiang,<sup>3</sup> S. Ciprini,<sup>14,15</sup> R. Claus,<sup>3</sup> J. Cohen-Tanugi,<sup>23</sup> J. Conrad,<sup>24,6,25,26</sup> H. Dereli,<sup>12</sup> C. D. Dermer,<sup>1</sup> A. de Angelis,<sup>27</sup> F. de Palma,<sup>16,17</sup> S. W. Digel,<sup>3</sup> G. Di Bernardo,<sup>7</sup> M. Dormody,<sup>4</sup> E. do Couto e Silva,<sup>3</sup> P. S. Drell,<sup>3</sup> R. Dubois,<sup>3</sup> D. Dumora,<sup>28,29</sup> Y. Edmonds,<sup>3</sup> C. Farnier,<sup>23</sup> C. Favuzzi,<sup>16,17</sup> S. J. Fegan,<sup>18</sup> W. B. Focke,<sup>3</sup> M. Frailis,<sup>27</sup> Y. Fukazawa,<sup>30</sup> S. Funk,<sup>3</sup> P. Fusco,<sup>16,17</sup> D. Gaggero,<sup>7</sup> F. Gargano,<sup>17</sup> N. Gehrels,<sup>22,31</sup> S. Germani,<sup>14,15</sup> B. Giebels,<sup>18</sup> N. Giglietto,<sup>16,17</sup> F. Giordano,<sup>16,17</sup> T. Glanzman,<sup>3</sup> G. Godfrey,<sup>3</sup> I. A. Grenier,<sup>8</sup> M.-H. Grondin,<sup>28,29</sup> J. E. Grove,<sup>1</sup> L. Guillemot,<sup>28,29</sup> S. Guiriec,<sup>32</sup> Y. Hanabata,<sup>30</sup> A. K. Harding,<sup>22</sup> M. Hayashida,<sup>3</sup> E. Hays,<sup>22</sup> R. E. Hughes,<sup>13</sup> G. Jóhannesson,<sup>3</sup> A. S. Johnson,<sup>3</sup> R. P. Johnson,<sup>4</sup> T. J. Johnson,<sup>22,31</sup> W. N. Johnson,<sup>1</sup> T. Kamae,<sup>3</sup> H. Katagiri,<sup>30</sup> J. Kataoka,<sup>33,34</sup> N. Kawai,<sup>33,35</sup> M. Kerr,<sup>19</sup> J. Knödlseeder,<sup>36</sup> M. L. Kocian,<sup>3</sup> F. Kuehn,<sup>13</sup> M. Kuss,<sup>7</sup> J. Lande,<sup>3</sup> L. Latronico,<sup>7</sup> F. Longo,<sup>9,10</sup> F. Loparco,<sup>16,17</sup> B. Lott,<sup>28,29</sup> M. N. Lovellette,<sup>1</sup> P. Lubrano,<sup>14,15</sup> G. M. Madejski,<sup>3</sup> A. Makeev,<sup>1,21</sup> M. N. Mazziotta,<sup>17</sup> W. McConville,<sup>22,31</sup> J. E. McEnery,<sup>22</sup> C. Meurer,<sup>24,6</sup> P. F. Michelson,<sup>3</sup> W. Mitthumsiri,<sup>3</sup> T. Mizuno,<sup>30</sup> A. A. Moiseev,<sup>37,31</sup> C. Monte,<sup>16,17</sup> M. E. Monzani,<sup>3</sup> A. Morselli,<sup>38</sup> I. V. Moskalenko,<sup>3</sup> S. Murgia,<sup>3</sup> P. L. Nolan,<sup>3</sup> E. Nuss,<sup>23</sup> T. Ohsugi,<sup>30</sup> A. Okumura,<sup>39</sup> N. Omodei,<sup>7</sup> E. Orlando,<sup>40</sup> J. F. Ormes,<sup>41</sup> D. Paneque,<sup>3</sup> J. H. Panetta,<sup>3</sup> D. Parent,<sup>28,29</sup> V. Pelassa,<sup>23</sup> M. Pepe,<sup>14,15</sup> M. Pesce-Rollins,<sup>7</sup> F. Piron,<sup>23</sup> T. A. Porter,<sup>4</sup> S. Rainò,<sup>16,17</sup> R. Rando,<sup>11,12</sup> M. Razzano,<sup>7</sup> A. Reimer,<sup>42,3</sup> O. Reimer,<sup>42,3</sup> T. Reposeur,<sup>28,29</sup> S. Ritz,<sup>4</sup> A. Y. Rodriguez,<sup>43</sup> M. Roth,<sup>19</sup> F. Ryde,<sup>25,6</sup> H. F.-W. Sadrozinski,<sup>4</sup> D. Sanchez,<sup>18</sup> A. Sander,<sup>13</sup> P. M. Saz Parkinson,<sup>4</sup> J. D. Scargle,<sup>44</sup> A. Sellerholm,<sup>24,6</sup> C. Sgrò,<sup>7</sup> D. A. Smith,<sup>28,29</sup> P. D. Smith,<sup>13</sup> G. Spandre,<sup>7</sup> P. Spinelli,<sup>16,17</sup> J.-L. Starck,<sup>8</sup> F. W. Stecker,<sup>22</sup> E. Striani,<sup>38,45</sup> M. S. Strickman,<sup>1</sup> A. W. Strong,<sup>40</sup> D. J. Suson,<sup>46</sup> H. Tajima,<sup>3</sup> H. Takahashi,<sup>30</sup> T. Tanaka,<sup>3</sup> J. B. Thayer,<sup>3</sup> J. G. Thayer,<sup>3</sup> D. J. Thompson,<sup>22</sup> L. Tibaldo,<sup>11,8,12</sup> D. F. Torres,<sup>47,43</sup> G. Tosti,<sup>14,15</sup> A. Tramacere,<sup>3,48</sup> Y. Uchiyama,<sup>49,3</sup> T. L. Usher,<sup>3</sup> V. Vasileiou,<sup>22,37,50</sup> N. Vilchez,<sup>36</sup> V. Vitale,<sup>38,45</sup> A. P. Waite,<sup>3</sup> P. Wang,<sup>3</sup> B. L. Winer,<sup>13</sup> K. S. Wood,<sup>1</sup> T. Ylinen,<sup>25,51,6</sup> and M. Ziegler<sup>4</sup>

(The Fermi LAT Collaboration)

<sup>1</sup>Space Science Division, Naval Research Laboratory, Washington, DC 20375, USA

<sup>2</sup>National Research Council Research Associate, National Academy of Sciences, Washington, DC 20001, USA

<sup>3</sup>W. W. Hansen Experimental Physics Laboratory,

Kavli Institute for Particle Astrophysics and Cosmology,

Department of Physics and SLAC National Accelerator Laboratory, Stanford University, Stanford, CA 94305, USA

<sup>4</sup>Santa Cruz Institute for Particle Physics, Department of Physics and Department of Astronomy and Astrophysics, University of California at Santa Cruz, Santa Cruz, CA 95064, USA

<sup>5</sup>Department of Astronomy, Stockholm University, SE-106 91 Stockholm, Sweden

<sup>6</sup>The Oskar Klein Centre for Cosmo Particle Physics, AlbaNova, SE-106 91 Stockholm, Sweden

<sup>7</sup>Istituto Nazionale di Fisica Nucleare, Sezione di Pisa, I-56127 Pisa, Italy

<sup>8</sup>Laboratoire AIM, CEA-IRFU/CNRS/Université Paris Diderot,

Service d'Astrophysique, CEA Saclay, 91191 Gif sur Yvette, France

<sup>9</sup>Istituto Nazionale di Fisica Nucleare, Sezione di Trieste, I-34127 Trieste, Italy

<sup>10</sup>Dipartimento di Fisica, Università di Trieste, I-34127 Trieste, Italy

<sup>11</sup>Istituto Nazionale di Fisica Nucleare, Sezione di Padova, I-35131 Padova, Italy

<sup>12</sup>Dipartimento di Fisica "G. Galilei", Università di Padova, I-35131 Padova, Italy

<sup>13</sup>Department of Physics, Center for Cosmology and Astro-Particle Physics,

The Ohio State University, Columbus, OH 43210, USA

<sup>14</sup>Istituto Nazionale di Fisica Nucleare, Sezione di Perugia, I-06123 Perugia, Italy

<sup>15</sup>Dipartimento di Fisica, Università degli Studi di Perugia, I-06123 Perugia, Italy

<sup>16</sup>Dipartimento di Fisica "M. Merlin" dell'Università e del Politecnico di Bari, I-70126 Bari, Italy

<sup>17</sup>Istituto Nazionale di Fisica Nucleare, Sezione di Bari, 70126 Bari, Italy

<sup>18</sup>Laboratoire Leprince-Ringuet, École polytechnique, CNRS/IN2P3, Palaiseau, France

<sup>19</sup>Department of Physics, University of Washington, Seattle, WA 98195-1560, USA

<sup>20</sup>INAF-Istituto di Astrofisica Spaziale e Fisica Cosmica, I-20133 Milano, Italy

<sup>21</sup>George Mason University, Fairfax, VA 22030, USA

<sup>22</sup>NASA Goddard Space Flight Center, Greenbelt, MD 20771, USA

- <sup>23</sup>Laboratoire de Physique Théorique et Astroparticules,  
Université Montpellier 2, CNRS/IN2P3, Montpellier, France
- <sup>24</sup>Department of Physics, Stockholm University, AlbaNova, SE-106 91 Stockholm, Sweden
- <sup>25</sup>Department of Physics, Royal Institute of Technology (KTH), AlbaNova, SE-106 91 Stockholm, Sweden
- <sup>26</sup>Royal Swedish Academy of Sciences Research Fellow,  
funded by a grant from the K. A. Wallenberg Foundation
- <sup>27</sup>Dipartimento di Fisica, Università di Udine and Istituto Nazionale di Fisica Nucleare,  
Sezione di Trieste, Gruppo Collegato di Udine, I-33100 Udine, Italy
- <sup>28</sup>Université de Bordeaux, Centre d'Études Nucléaires Bordeaux Gradignan, UMR 5797, Gradignan, 33175, France
- <sup>29</sup>CNRS/IN2P3, Centre d'Études Nucléaires Bordeaux Gradignan, UMR 5797, Gradignan, 33175, France
- <sup>30</sup>Department of Physical Sciences, Hiroshima University, Higashi-Hiroshima, Hiroshima 739-8526, Japan
- <sup>31</sup>University of Maryland, College Park, MD 20742, USA
- <sup>32</sup>University of Alabama in Huntsville, Huntsville, AL 35899, USA
- <sup>33</sup>Department of Physics, Tokyo Institute of Technology, Meguro City, Tokyo 152-8551, Japan
- <sup>34</sup>Waseda University, 1-104 Totsukamachi, Shinjuku-ku, Tokyo, 169-8050, Japan
- <sup>35</sup>Cosmic Radiation Laboratory, Institute of Physical and Chemical Research (RIKEN), Wako, Saitama 351-0198, Japan
- <sup>36</sup>Centre d'Étude Spatiale des Rayonnements, CNRS/UPS, BP 44346, F-30128 Toulouse Cedex 4, France
- <sup>37</sup>Center for Research and Exploration in Space Science and Technology (CRESTT),  
NASA Goddard Space Flight Center, Greenbelt, MD 20771, USA
- <sup>38</sup>Istituto Nazionale di Fisica Nucleare, Sezione di Roma "Tor Vergata", I-00133 Roma, Italy
- <sup>39</sup>Department of Physics, Graduate School of Science,  
University of Tokyo, 7-3-1 Hongo, Bunkyo-ku, Tokyo 113-0033, Japan
- <sup>40</sup>Max-Planck Institut für extraterrestrische Physik, 85748 Garching, Germany
- <sup>41</sup>Department of Physics and Astronomy, University of Denver, Denver, CO 80208, USA
- <sup>42</sup>Institut für Astro- und Teilchenphysik and Institut für Theoretische Physik,  
Leopold-Franzens-Universität Innsbruck, A-6020 Innsbruck, Austria
- <sup>43</sup>Institut de Ciències de l'Espai (IEEC-CSIC), Campus UAB, 08193 Barcelona, Spain
- <sup>44</sup>Space Sciences Division, NASA Ames Research Center, Moffett Field, CA 94035-1000, USA
- <sup>45</sup>Dipartimento di Fisica, Università di Roma "Tor Vergata", I-00133 Roma, Italy
- <sup>46</sup>Department of Chemistry and Physics, Purdue University Calumet, Hammond, IN 46323-2094, USA
- <sup>47</sup>Institució Catalana de Recerca i Estudis Avançats, Barcelona, Spain
- <sup>48</sup>Consorzio Interuniversitario per la Fisica Spaziale (CIFS), I-10133 Torino, Italy
- <sup>49</sup>Institute of Space and Astronautical Science, JAXA,  
3-1-1 Yoshinodai, Sagami-hara, Kanagawa 229-8510, Japan
- <sup>50</sup>University of Maryland, Baltimore County, Baltimore, MD 21250, USA
- <sup>51</sup>School of Pure and Applied Natural Sciences, University of Kalmar, SE-391 82 Kalmar, Sweden
- (Dated: October 24, 2018)

The diffuse Galactic  $\gamma$ -ray emission is produced by cosmic rays (CRs) interacting with the interstellar gas and radiation field. Measurements by the Energetic Gamma-Ray Experiment Telescope (EGRET) instrument on the *Compton Gamma-Ray Observatory* indicated excess  $\gamma$ -ray emission  $\gtrsim 1$  GeV relative to diffuse Galactic  $\gamma$ -ray emission models consistent with directly measured CR spectra (the so-called "EGRET GeV excess"). The excess emission was observed in all directions on the sky, and a variety of explanations have been proposed, including beyond-the-Standard-Model scenarios like annihilating or decaying dark matter. The Large Area Telescope (LAT) instrument on the *Fermi* Gamma-ray Space Telescope has measured the diffuse  $\gamma$ -ray emission with improved sensitivity and resolution compared to EGRET. We report on LAT measurements of the diffuse  $\gamma$ -ray emission for energies 100 MeV to 10 GeV and Galactic latitudes  $10^\circ \leq |b| \leq 20^\circ$ . The LAT spectrum for this region of the sky is well reproduced by a diffuse Galactic  $\gamma$ -ray emission model that is consistent with local CR spectra and inconsistent with the EGRET GeV excess.

PACS numbers: 95.30.Cq,95.55.Ka,95.85.Pw,96.50.sb,98.70.Sa

*Introduction:* The diffuse  $\gamma$ -ray emission, both Galactic and extragalactic, is of significant interest for astrophysics, particle physics, and cosmology. The diffuse Galactic emission (DGE) is produced by interactions of cosmic rays (CRs), mainly protons and electrons, with the interstellar gas (via  $\pi^0$ -production and bremsstrahlung) and radiation field (via inverse Compton [IC] scattering) [1, 2]. It is a direct probe of CR fluxes in distant locations, and may contain signatures of physics

beyond the Standard Model, such as dark matter annihilation or decay. The DGE is a foreground for point-source detection and hence influences the determination of the source positions and fluxes. It is also a foreground for the much fainter extragalactic component, which is the sum of contributions from unresolved sources and truly diffuse emission, including any signatures of large scale structure formation, emission produced by ultra-high-energy CRs interacting with relic photons, and many other processes

(e.g., [3] and references therein). Therefore, understanding the DGE is a necessary first step in all such studies.

The excess diffuse emission  $\gtrsim 1$  GeV in the Energetic Gamma-Ray Experiment Telescope (EGRET) data [4] relative to that expected from DGE models consistent with the directly measured CR nucleon and electron spectra [4, 5] led to the proposal that this emission was the long-awaited signature of dark matter annihilation [6]. More conventional interpretations included variations of CR spectra in the Galaxy [4, 5, 7], contributions by unresolved point sources [8], and instrumental effects [4, 9, 10].

A model of the DGE depends on the CR spectra throughout the Galaxy as well as the distribution of the target gas and interstellar radiation field (ISRF). Starting from the distribution of CR sources and particle injection spectra, the distribution of CRs throughout the Galaxy is determined taking into account relevant energy losses and gains, then the CR distributions are folded with the target distributions to calculate the DGE [e.g., 11]. Defining the inputs and calculating the models are not trivial tasks and involve analysis of data from a broad range of astronomical and astroparticle instruments [12].

The *Fermi* Large Area Telescope (LAT) was launched on June 11, 2008. It is over an order of magnitude more sensitive than its predecessor, EGRET, with a more stable response due to the lack of consumables. The LAT data permit more detailed studies of the DGE than have been possible ever before.

In this paper, analysis and results for the DGE are shown for the Galactic mid-latitude range  $10^\circ \leq |b| \leq 20^\circ$  measured by the LAT in the first 5 months of the science phase of the mission. This region was chosen for initial study since it maximises the fraction of signal from DGE produced within several kpc of the Sun and hence uncertainties associated with CR propagation, knowledge of the gas distribution, etc., should be minimised. The calculation of the DGE at lower Galactic latitudes requires CR fluxes throughout the whole Galaxy and thus is model dependent, while the emission at higher latitudes is more affected by contamination from charged particles misclassified as photons and uncertainties in the model used to estimate the DGE. The diffuse emission at lower and higher Galactic latitudes will be addressed in subsequent LAT papers.

*LAT Data Selection and Analysis:* The LAT is a pair-conversion telescope with a precision tracker and calorimeter, each consisting of a  $4 \times 4$  array of 16 modules, a segmented anti-coincidence detector (ACD) that covers the tracker array, and a programmable trigger and data acquisition system. Full details of the instrument, onboard and ground data processing, and other mission-oriented support are given in [13].

The data selection used in this paper is made using the standard LAT ground processing and background rejection scheme [13]. This consists of two basic parts: first

a simple accept-or-reject selection (prefiltering) followed by a classification tree (CT) [14] based determination of the relative probability of being background or signal. The prefiltering phase screens particles entering the LAT for their charge neutrality using the tracker and ACD. The direction reconstruction software extrapolates particle trajectories found in the tracker back to the scintillation tiles of the ACD, and we accept only events in which the intersected tiles show no significant signal. In addition, the prefiltering phase includes considerations of the shape of the calorimeter shower energy deposition and how well the found tracks project into the energy centroid. The overall background rejection of the prefiltering phase is  $10^3 - 10^4$  depending on energy, yielding an efficiency  $> 90\%$  for  $\gamma$ -rays that convert into electron-positron pairs in the LAT.

Classification trees, which afford an efficient and statistically robust method for distinguishing signal from noise, are used to reduce backgrounds further. Using quantities defined from ACD, tracker, and calorimeter data, the CTs are trained on Monte Carlo simulated data which have passed the prefilter described above. Multiple CTs are built to make the procedure robust against statistical fluctuations during the training procedure. The result from averaging the output from these CTs is the probability for an event to be a photon or background. This final selection parameter allows the signal purity to be set according to the needs of the analysis. For the analysis of diffuse emission, the cut on the CT generated probability is set such that the Monte Carlo prediction of the orbit-averaged background rate is  $\sim 0.1$  Hz integrated over the full instrument acceptance  $> 100$  MeV. This yields a  $\gamma$ -ray efficiency  $> 80\%$ , and the residual background is at a level where the majority of the contamination arises from irreducible sources such as  $\gamma$ -rays produced by CR interactions in the passive material outside the ACD, e.g., the thermal blanket and micrometeoroid shield of the LAT (see Fig. 13 in [13]). The events corresponding to the above criterion are termed “Diffuse” class and are the standard low-background event selection.

The analysis presented here uses post-launch instrument response functions (IRFs). These take into account pile-up and accidental coincidence effects in the detector subsystems that are not considered in the definition of the pre-launch IRFs. Cosmic rays, primarily protons, pass through the LAT at a high rate and sufficiently near coincidences with  $\gamma$ -rays leave residual signals that can result in  $\gamma$ -rays being misclassified, particularly at energies  $\lesssim 300$  MeV. The post-launch IRFs were derived using LAT events read from a special trigger that produces periodic detector readouts, irrespective of the signals present, as a background overlay on the standard simulations of  $\gamma$ -rays and provide an accurate accounting for the instrumental pile-up and accidental coincidence effects. The on-axis effective area for the event selection

used in this paper is  $\sim 7000 \text{ cm}^2$  at 1 GeV and is energy dependent; this is approximately 10% lower at 1 GeV than the pre-launch effective area corresponding to the same event selection. The systematic uncertainties of the effective area, evaluated by comparing the efficiencies of analysis cuts for data and simulation of observations of Vela, are also energy dependent: 10% below 100 MeV, decreasing to 5% at 560 MeV, and increasing to 20% at 10 GeV and above. The point spread function (PSF) and energy resolution are as described in [13].

The LAT nominally operates in a scanning mode that covers the whole sky every two orbits (i.e., 3 hrs). We use data taken in this mode from the commencement of scientific operations in mid-August 2008 to the end of December 2008. The data were prepared using the LAT Science Tools package, which is available from the *Fermi* Science Support Center [15]. Events satisfying the Diffuse class selection and coming from zenith angles  $< 105^\circ$  (to greatly reduce the contribution by Earth albedo  $\gamma$ -rays) were used. To further reduce the effect of Earth albedo backgrounds, the time intervals when the Earth was appreciably within the field of view (specifically, when the centre of the field of view was more than  $47^\circ$  from the zenith) were excluded from this analysis. This leaves 9.83 Ms of total livetime in the data set. The energy-dependent exposure was calculated using the IRFs described above.

The photon counts and exposure were further processed using the *GaRDian* package, part of a suite of tools we have developed to analyse the DGE where the analysis approach is described in [16], with more details to be given in a subsequent publication. Gamma-ray skymaps were generated using a HEALPix [17] scheme at order 7 (i.e.,  $\sim 0.2^\circ$  resolution) with 5 bins per decade in energy from 100 MeV to 10 GeV. For each energy bin the intensity was obtained by dividing the in-bin counts by the spectrally-weighted exposure over the bin. We used two methods for the spectral weighting: a power law with index  $-2$  and the spectral shape of the assumed DGE model (described below). With the energy binning used in this paper the differences in the derived intensities were  $< 1\%$  between these two weighting schemes.

Figure 1 shows the LAT data averaged over all Galactic longitudes and the latitude range  $10^\circ \leq |b| \leq 20^\circ$ . The hatched band surrounding the LAT data indicates the systematic uncertainty in the measurement due to the uncertainty in the effective area described above. Also shown are the EGRET data for the same region of sky derived from count maps and exposures available via the *CGRO* Science Support Center [18] and processed following the procedure described in [11] and we have included the standard systematic uncertainty of 13% [19]. For both data sets the contribution by point sources has not been subtracted. The LAT-measured spectrum is significantly softer than the EGRET measurement with an integrated intensity  $J_{\text{LAT}}(\geq 1 \text{ GeV}) = 2.35 \pm 0.01 \times 10^{-6}$

$\text{cm}^{-2} \text{ s}^{-1} \text{ sr}^{-1}$  compared to the EGRET integrated intensity  $J_{\text{EGRET}}(\geq 1 \text{ GeV}) = 3.16 \pm 0.05 \times 10^{-6} \text{ cm}^{-2} \text{ s}^{-1} \text{ sr}^{-1}$  where the errors are statistical only. Not included in the figure is the systematic uncertainty in the energy scale, which is conservatively estimated from comparison between Monte Carlo and beam test data as  $< 5\%$  for 100 MeV to 1 GeV, and  $< 7\%$  above 1 GeV where it is believed that if any bias is present energies are overestimated. Taking the uncertainty on the energy scale into account, the LAT spectrum could be softer, increasing the discrepancy with the EGRET spectrum further.

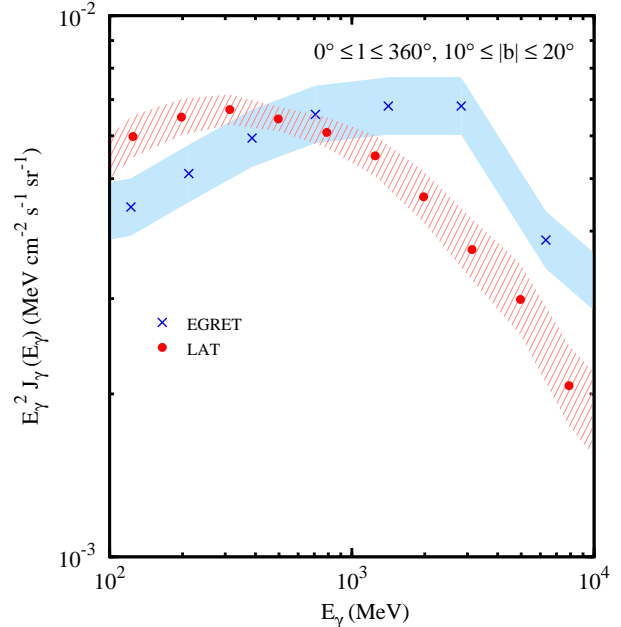


FIG. 1: Diffuse emission intensity averaged over all Galactic longitudes for latitude range  $10^\circ \leq |b| \leq 20^\circ$ . Data points: LAT, red dots; EGRET, blue crosses. Systematic uncertainties: LAT, red; EGRET, blue.

Figure 2 compares the LAT spectrum shown in Fig. 1 with the spectra of an *a priori* DGE model, and a point-source contribution and unidentified background (UIB) component derived from fitting the LAT data that are described below. The DGE model is an updated version of the “conventional” model from GALPROP [11]. Major improvements include use of the formalism and corresponding code for pion production in  $pp$ -interactions by [20], a complete recalculation of the ISRF [21], updated gas maps, and an improved line-of-sight integration routine. However, it is still an *a priori* model that is based on local cosmic-ray data, and does not use  $\gamma$ -ray data. Table I summarises the numerical values by energy bin for the different components shown in Fig. 2.

The source and UIB components were obtained by fitting the LAT data using *GaRDian* with the DGE model held constant. Point source locations were taken from the 3 month *Fermi* LAT source list down to sources with

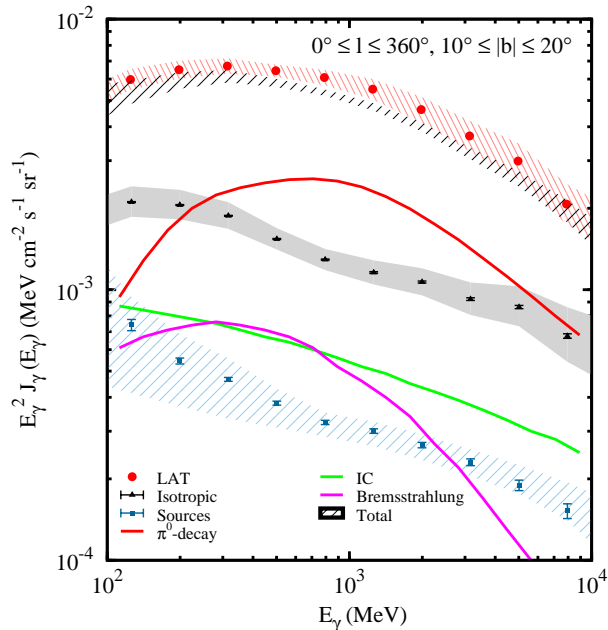


FIG. 2: LAT data with model, source, and UIB components for sky region in Fig. 1. Model (lines):  $\pi^0$ -decay, red; bremsstrahlung, magenta; IC, green. Shaded/hatched regions: UIB, grey/solid; source, blue/hatched; total (model + UIB + source), black/hatched.

5- $\sigma$  significance. Due to the limited statistics of all but the very brightest sources, we used 3 bins per energy decade in the fitting procedure. Source positions were fixed but the spectra were fit using one free parameter for the source flux per energy bin. The UIB component was determined by fitting the data and sources over all Galactic longitudes for the high-latitude region  $|b| \geq 30^\circ$  for the full LAT energy range shown in the figure. Using this high-latitude region minimises the effect of contamination by the bright Galactic ridge which can be significant even up to  $\sim 10^\circ$  from the plane due to the long tails of the PSF at low energies.

To determine the uncertainty of the source and UIB components, we modified the effective area to the extremes of its systematic uncertainty defined before and refitted the data. Since the DGE model components do not vary in the fit, the absolute change in intensity caused by the modification to the effective area propagates directly to the source and UIB components. The systematic uncertainty on these components is energy dependent and due to several effects.

For energies  $\gtrsim 10$  GeV the PSF is  $\sim 0.2^\circ$  (68% containment) and the sources are well-localised spatially. Since the model is fixed and the sky maps are sparser at high latitudes for the data taking period in this paper, the UIB component absorbs almost all of the intensity from the modification to the effective area. At low energies the PSF is wider,  $3.5^\circ$  (68% containment) at 100 MeV

TABLE I: LAT data and components:  $10^\circ \leq |b| \leq 20^\circ$ .

Energy <sup>a</sup>	LAT <sup>b,e</sup>	Model <sup>b,c,d</sup>				UIB <sup>b,e,f</sup>		Source <sup>b,e</sup>
100–158	$59.8 \pm 0.3$	26.0	11.0	6.4	8.6	$21.0 \pm 0.1$	$7.4 \pm 0.4$	
158–251	$65.0 \pm 0.3$	33.5	18.2	7.3	8.0	$20.5 \pm 0.1$	$5.4 \pm 0.1$	
251–398	$67.1 \pm 0.3$	38.2	23.2	7.6	7.4	$18.7 \pm 0.1$	$4.7 \pm 0.1$	
398–631	$64.5 \pm 0.3$	38.9	25.3	7.0	6.6	$15.4 \pm 0.1$	$3.8 \pm 0.1$	
631–1000	$60.8 \pm 0.3$	37.3	25.7	5.7	5.9	$12.9 \pm 0.1$	$3.2 \pm 0.1$	
1000–1585	$55.1 \pm 0.4$	32.8	23.3	4.4	5.1	$11.6 \pm 0.1$	$3.0 \pm 0.1$	
1585–2512	$46.3 \pm 0.4$	26.5	19.0	3.1	4.4	$10.7 \pm 0.1$	$2.7 \pm 0.1$	
2512–3981	$37.0 \pm 0.5$	20.2	14.4	2.0	3.8	$9.2 \pm 0.1$	$2.3 \pm 0.1$	
3981–6310	$29.9 \pm 0.5$	14.9	10.5	1.2	3.2	$8.5 \pm 0.1$	$1.9 \pm 0.1$	
6310–10000	$20.7 \pm 0.5$	10.9	7.5	0.7	2.7	$6.8 \pm 0.1$	$1.5 \pm 0.1$	

<sup>a</sup>MeV

<sup>b</sup> $E_\gamma^2 J(E_\gamma)$  ( $10^{-4}$  MeV cm $^{-2}$  s $^{-1}$  sr $^{-1}$ ) evaluated at the mid-bin energy.

<sup>c</sup>Total/ $\pi^0$ -decay/bremsstrahlung/inverse Compton.

<sup>d</sup>The GALPROP galdef ID for this model is 54\_5gXvarh7S which is available at the website <http://galprop.stanford.edu>.

<sup>e</sup>Statistical errors only.

<sup>f</sup>Unidentified background.

for  $\gamma$ -ray conversions in the front section of the LAT, and the sources are less well-localised spatially. In addition, the sky maps are well populated even at high latitudes and display spatial structure. The PSF broadening of the sources provides spatial structure and because the DGE model is fixed, more intensity is assigned to the source component to compensate in the fit. These effects lead to the systematic error in the source component being relatively larger than the isotropic at low energies and vice versa at high energies. Note, this applies for the high-latitude region from where the UIB component is derived, and also for the mid-latitude range for which we show the combined contribution by sources in Fig. 2. Because the uncertainties in the source and UIB components are not independent we have conservatively added their systematic uncertainties for the total intensity band shown in Fig. 2.

The UIB component comprises the true extragalactic diffuse  $\gamma$ -ray emission, emission from unresolved Galactic and extragalactic sources, and residual particle backgrounds (CRs that pass the  $\gamma$ -ray classification analysis and  $\gamma$ -rays produced by CR interactions in the passive material outside the ACD) in the LAT data. In addition, other relevant foreground components that are not completely modelled, such as emission from the solar disk and extended emission [22] and other potentially relevant “diffuse” sources [23] are included. Hence, the UIB component does *not* constitute a measurement of the extragalactic diffuse emission. Furthermore, comparison with the EGRET estimate of the extragalactic diffuse emission [24] is problematic due to the different DGE models used and analysis details that are beyond the scope of the current paper and will be addressed in a subsequent publication [25].

*Discussion:* The intensity scales of the LAT and

EGRET have been found to be different with the result that the LAT-measured spectra are softer. In our early study of the Vela spectrum [26], which was made using pre-launch IRFs, the difference was apparent already above 1 GeV. Following on-orbit studies new IRFs have been developed to account for inefficiencies in the detection of  $\gamma$ -rays in the LAT due to pile-up and accidental coincidence effects in the detector subsystems. The inefficiency increases at lower energies, with the result that the IRFs used in the present analysis indicate greater intensities in the range below 1 GeV, with the magnitude of the effect ranging up to  $\sim 30\%$  at 100 MeV. A forthcoming study of the Vela pulsar using the LAT one-year data with post-launch IRFs also shows a similar effect in the low-energy pulsed spectrum. So, the relative brightness of the diffuse emission measured by the LAT at low energies is unlikely to be due to increased residual background. Our confidence that the IRFs used in the present analysis accurately represent our knowledge of the instrument comes from detailed instrument simulations that were validated with beam tests of calibration units, and to post-launch refinements based on actual particle backgrounds. The systematic uncertainty on the effective area gives an energy dependent measure of our confidence in the IRFs used in the present analysis.

As a consequence, the LAT-measured DGE spectrum averaged over all Galactic longitudes for the latitude range  $10^\circ \leq |b| \leq 20^\circ$  is systematically softer than the EGRET-measured spectrum. The spectral shape is compatible with that of an *a priori* DGE model that is consistent with directly measured CR spectra. The excess emission above 1 GeV measured by EGRET is not seen by the LAT in this region of the sky.

While the LAT spectral shape is consistent with the DGE model used in this paper, the overall model emission is too low thus giving rise to a  $\sim 10 - 15\%$  excess over the energy range 100 MeV to 10 GeV. However, the DGE model is based on pre-*Fermi* data and knowledge of the DGE. The difference between the model and data is of the same order as the uncertainty in the measured CR nuclei spectra at the relevant energies [27]. In addition, other model parameters that can affect the  $\gamma$ -ray production rate (e.g., the conversion between CO line intensity and molecular hydrogen column density in the interstellar medium,  $X_{\text{CO}}$ ) have not been modified in the present paper. Overall, the agreement between the LAT-measured spectrum and the model shows that the fundamental processes are consistent with our data, thus providing a solid basis for future work understanding the DGE.

*Acknowledgements:* The *Fermi* LAT Collaboration acknowledges support from a number of agencies and institutes for both development and the operation of the LAT as well as scientific data analysis. These include

NASA and DOE in the United States, CEA/Irfu and IN2P3/CNRS in France, ASI and INFN in Italy, MEXT, KEK, and JAXA in Japan, and the K. A. Wallenberg Foundation, the Swedish Research Council and the National Space Board in Sweden. Additional support from INAF in Italy for science analysis during the operations phase is also gratefully acknowledged.

GALPROP development is partially funded via NASA grant NNX09AC15G.

Some of the results in this paper have been derived using the HEALPix [17] package.

- 
- [1] V. L. Ginzburg and S. I. Syrovatskii, *The Origin of Cosmic Rays* (Macmillan, New York, 1964).
  - [2] F. W. Stecker, NASA Special Publication **249** (1971).
  - [3] C. D. Dermer, in *The 1st GLAST Symposium*, edited by S. Ritz, et al. (2007), vol. 921 of *AIP Conf. Ser.*, pp. 122–126.
  - [4] S. D. Hunter et al., *Astrophys. J.* **481**, 205 (1997).
  - [5] A. W. Strong, I. V. Moskalenko, and O. Reimer, *Astrophys. J.* **537**, 763 (2000).
  - [6] W. de Boer et al., *Astron. & Astrophys.* **444**, 51 (2005).
  - [7] T. A. Porter and R. J. Protheroe, *J. Phys. G* **23**, 1765 (1997).
  - [8] E. G. Berezhko and H. J. Völk, *Astrophys. J.* **611**, 12 (2004).
  - [9] I. V. Moskalenko et al., *Nucl. Phys. B Proc. Suppl.* **173**, 44 (2007).
  - [10] F. W. Stecker, S. D. Hunter, and D. A. Kniffen, *Astropart. Phys.* **29**, 25 (2008).
  - [11] A. W. Strong, I. V. Moskalenko, and O. Reimer, *Astrophys. J.* **613**, 962 (2004).
  - [12] A. W. Strong, I. V. Moskalenko, and V. S. Ptuskin, *Annu. Rev. Nucl. Part. Sci.* **57**, 285 (2007).
  - [13] W. B. Atwood et al., *Astrophys. J.* **697**, 1071 (2009).
  - [14] L. Breiman et al., *Classification and Regression Trees* (Wadsworth International Group, Belmont CA, 1984).
  - [15] <http://fermi.gsfc.nasa.gov/ssc>.
  - [16] M. Ackermann et al., in *Proceedings of the 4th International Meeting on High Energy Gamma-Ray Astronomy*, edited by F. A. Aharonian, et al. (2008), vol. 1085 of *AIP Conf. Ser.*, pp. 763–766.
  - [17] K. M. Górski et al., *Astrophys. J.* **622**, 759 (2005).
  - [18] <http://heasarc.gsfc.nasa.gov/docs/cgro/egret/>.
  - [19] J. A. Esposito et al., *Astrophys. J. Supp.* **123**, 203 (1999).
  - [20] T. Kamae et al., *Astrophys. J.* **647**, 692 (2006).
  - [21] T. A. Porter et al., *Astrophys. J.* **682**, 400 (2008).
  - [22] I. V. Moskalenko, T. A. Porter, and S. W. Digel, *Astrophys. J. Lett.* **652**, L65 (2006).
  - [23] I. V. Moskalenko and T. A. Porter, *Astrophys. J.* **670**, 1467 (2007).
  - [24] P. Sreekumar et al., *Astrophys. J.* **494**, 523 (1998).
  - [25] A. A. Abdo et al., *Phys. Rev. Lett.* (submitted) (2009).
  - [26] A. A. Abdo et al., *Astrophys. J.* **696**, 1084 (2009).
  - [27] Y. Shikaze et al., *Astropart. Phys.* **28**, 154 (2007).